Journal of Structural Biology xxx (2017) xxx–xxx

Contents lists available at ScienceDirect

Journal of Structural Biology

journal homepage: www.elsevier.com/locate/yjsbi

A direct-imaging cryo-EM study of shedding extracellular vesicles from leukemic monocytes

Na'ama Koifman [a], Idan Biran [a], Anat Aharon [b,c], Benjamin Brenner [b,c], Yeshayahu Talmon [a,*]

[a] Department of Chemical Engineering and the Russell Berrie Nanotechnology Institute, Technion-Israel Institute of Technology, Haifa 3200003, Israel
[b] The Bruce Rappaport Faculty of Medicine, Technion-Israel Institute of Technology, Haifa 3525433, Israel
[c] Department of Hematology and Bone Marrow Transplantation, Rambam Health Care Campus, Haifa 3109601, Israel

ARTICLE INFO

Article history:
Received 6 October 2016
Received in revised form 9 February 2017
Accepted 14 February 2017
Available online xxxx

Keywords:
Cryo-EM
Cell stimulation
Endotoxins
Microparticles
Blebbing
NTA

ABSTRACT

The human leukemia monocytic cell line (THP-1) is known to shed extracellular vesicles (EVs) under various stimulations. We studied the effects of two types of common stimulation types, lipopolysaccharide (LPS) and starvation conditions by high resolution cryogenic electron microscopy, namely, cryo-SEM and cryo-TEM. Cryo-SEM data of cells undergoing EV blebbing and shedding is presented here for the first time. The high-resolution images show good agreement with models describing the membrane processes of shedding. Cells that underwent a 48-h starvation treatment exhibited differing morphological features, including shrunken nucleus and elongated membrane protrusions. LPS treated cells, however, showed extensive blebbing originating from the cell membrane, in good agreement with the sizes of EVs imaged by cryo-TEM. EVs isolated from both types of stimulations were measured by nanoparticle tracking analysis (NanoSight), by which LPS-EVs samples exhibited higher concentration and smaller mean diameter, as compared to starvation-EVs. Our results suggest a difference in the effects of the two stimulation types on the shedding process and possibly on the type of EVs shed. Our unique methodologies provide an important and innovative outlook of the shedding process and on its products, paving the way to further discoveries in this developing field of research, in which much is still unknown.

1. Introduction

Extracellular vesicles (EVs) are shed from a variety of cell lines in a process that is rarely investigated by direct imaging means. This is mostly owing to their relatively heterogeneous size, ranging from as small as tens of nanometers up to several micrometers. Under the general term of EVs we include cell-membrane shed microparticles, exosomes and apoptotic bodies, which are similar in structure but differ in their release mechanism, function and size (Gould and Raposo, 2013; Hargett and Bauer, 2013; Heijnen et al., 1999; Piccin et al., 2007; Théry et al., 2002). Depending on their type and source, EVs are released carrying a variety of cellular components from their cell of origin. These include membrane proteins, bioactive lipids, genetic material (mRNA, miRNA, DNA), and possibly also cell organelles (Hugel et al., 2005; Katsuda et al., 2014; Sturk and Nieuwland, 2012). Thus they are involved in various processes such as coagulation, cell-to-cell communication, inflammation, apoptosis, angiogenesis, immune suppression, and cell migration and transformation (Castellana et al., 2010; Cocucci et al., 2009; Hugel et al., 2005; Meziani et al., 2008; Redman and Sargent, 2007; Shai and Varon, 2011; Sturk and Nieuwland, 2012). Although they are released under normal physiological conditions in the body, their concentration rises significantly during pregnancy (Redman and Sargent, 2007) and pregnancy related complications such as preeclampsia (Redman and Sargent, 2007; Shomer et al., 2013), and certain pathophysiological conditions, including, cardiovascular diseases (Meziani et al., 2008), diabetes (Chahed et al., 2010; Tsimerman et al., 2011), and various types of cancer (Castellana et al., 2010; Katsuda et al., 2014; Minciacchi et al., 2015a; Shedden et al., 2003).

THP1 is a cell line of acute leukemic monocytes, and is also found among the cells known for their ability to shed extracellular vesicles upon stimulation. Because of its high expression of CD14, the homing receptor for lipopolysaccharide (LPS), an effective stimulation for THP1 cells is by incubation with LPS, an endotoxin known for its ability to initiate an immune response in various eukaryotic organisms. In mammalian species, it specifically targets the phagocytes of innate immunity, including monocytes, macrophages and neutrophils (Alexander and Rietschel, 2001). Among the responses initiated by LPS on THP1, is the shedding of extracellular vesicles (EVs) (Aharon et al., 2008).

* Corresponding author.
E-mail address: ishi@technion.ac.il (Y. Talmon).

http://dx.doi.org/10.1016/j.jsb.2017.02.004
1047-8477/

Microparticles originate in the cell membrane, and are released in a shedding process; exosomes are produced in the cytoplasm, and are released by exocytosis from multivesicular bodies (MVBs) and apoptotic bodies are large vesicles (~800 nm to 5 μm in diameter) released by the cell as it undergoes programmed cell death (Hargett and Bauer, 2013; Heijnen et al., 1999; Piccin et al., 2007; Théry et al., 2002). Another class of EVs are large oncosomes, shed specifically from cancerous cells (Minciacchi et al., 2015a, 2015b).

According to one of the key models presented by Piccin et al. (Piccin et al., 2007), the shedding process is activated by stimulation of the cell, initiating a calcium-dependent process, in turn leading to inhibition of enzymes that are responsible for the maintenance of membrane asymmetry and proteolysis of cytoskeletal filaments, resulting in membrane cleavage. The disruption of asymmetry leads to migration of phosphatidylserine (PS), composing mainly the inner leaflet of the plasma membrane, to the outer leaflet. That increases membrane curvature owing to PS negatively-charged head groups, forming a structure known as a bleb, which is finally pinched off as an extracellular vesicle (Piccin et al., 2007). This model, however, is based on a mechanism in platelets, and may not fit well other cell types and all classes of EVs.

We differentiate between shedding and blebbing, where the former is the process of releasing EVs from the cell to its surroundings, while the latter is the stage of EVs production during which they are still attached to the cell-membrane. To initiate the shedding process in cells, one can apply different types of stimulations, including incubation with endotoxins, starvation conditions (Aharon et al., 2008), and oxidative stress (Eldh et al., 2010; Hedlund et al., 2011).

EVs are fairly heterogeneous in size, ranging from a few tens of nanometers to several micrometers in diameter, thus, most techniques used for their study can detect and analyze only a certain fraction of the whole range of existing vesicles. Such techniques include flow cytometry (Crompot et al., 2015; Katzenell et al., 2012; van der Pol et al., 2014), nanoparticle tracking analysis (Dragovic et al., 2011; Gercel-Taylor et al., 2012), and dynamic light scattering (van Der Pol et al., 2010), which can provide information regarding size, concentration, and even composition, if fluorescent probes are used, but are limited in terms of their range of detection, and provide no morphological information. Direct imaging of EVs and cells undergoing blebbing and shedding has been achieved mostly by low resolution techniques, such as confocal and fluorescent microscopy, resulting in a fairly limited view in terms of size and detail (van Der Pol et al., 2010). Thus, the only technique that studies the particles individually and at a high enough resolution to resolve their structure is electron microscopy (EM), and more specifically, cryogenic-temperature electron microscopy, which is superior to room-temperature EM in the quality of liquid samples preservation prior to imaging (Arraud et al., 2014; Issman et al., 2013). Studying the shedding process by direct visualization is also limited in the literature to light and fluorescent microscopy, which can identify fairly large (μm to mm) vesicles at a low magnification and limited resolution (Atkin-Smith et al., 2015; Jaiswal et al., 2013; Lai et al., 2015; Minciacchi et al., 2015b; Zomer et al., 2015). This calls for a high resolution technique, which can reveal the entire range of membrane shedding at its different stages. We present here our work on THP1 cells undergoing blebbing and shedding, by cryogenic scanning electron microscopy (cryo-SEM), a technique that allows excellent preservation of cellular structures without chemical alterations, together with high-resolution imaging of the preserved structures. We complement our cryo-SEM work with cryogenic transmission electron microscopy of the shed EVs, as well as statistical data collected by nanoparticle tracking analysis (NTA), which revealed some interesting differences between EV population that were produced by different stimulation types. The combination of high-resolution direct imaging techniques establishes a detailed view of the shedding process occurring on cells, as well as on the shed EVs and their heterogeneous nature.

2. Experimental

2.1. Cell culture and EVs isolation

Cells were cultured in RPMI medium (Sigma Aldrich) supplemented with 10% fetal calf serum, 1% L-glutamine and 1% penicillin streptomycin (Biological Industries Beit Ha'Emek, Israel). Stimulation of cell blebbing and EVs production was induced by either incubation with lipopolysaccharide from Escherichia coli O111: B4 (1 μg/mL; Sigma Aldrich, St Louis, MO, USA) for 3 to 16 h, at 37 °C, or by 24–48 of incubation in serum-free medium, aka starvation conditions. Cells tested mycoplasma free throughout the procedures. Stimulation was applied to cells found on the same passage and to the same number of cells for control purposes. In addition, prior to LPS incubation cells were washed to verify that any isolated EV originated only from LPS stimulation.

EVs isolation was performed by multiple centrifugations: Following one of either stimulation types, cells with medium were collected and centrifuged twice at 1500 RPM for 10 min at 4 °C, to remove cells and cellular debris. Supernatant was collected and centrifuged at 20,000*g* for 1 h at 4 °C. The supernatant was discarded, and the pellet was re-suspended in phosphate buffer saline (PBS). The concentration factor of the 20,000*g* step is 60 (volume before/after centrifugation). Aliquots were rapidly frozen in liquid nitrogen according to recommendations by Issman et al. (Issman et al., 2013) and kept at −80 °C. Prior to investigation, EVs were rapidly thawed at 37 °C.

2.2. Cryo-SEM specimen preparation and imaging

For cryogenic scanning electron microscopy (cryo-SEM) imaging we used a Zeiss Ultra Plus high-resolution SEM, equipped with a Schottky field-emission gun and with a BalTec VCT100 cold-stage maintained below −145 °C. Specimens were imaged at low acceleration voltages of 1–1.2 kV, and working distances of 3–5 mm. We used both the Everhart Thornley ("SE2") and the in-the-column ("InLens") secondary electron imaging detectors. Low-dose imaging was applied to all specimens to minimize radiation damages.

Cells in RPMI medium were cryo-fixed by either high-pressure freezing (HPF), or by manual drop plunging. In the HPF technique, 1–3 μL of suspended cells were sandwiched between two metal discs (3 mm diameter, 50 μm cavities), and were then high-pressure frozen (HPM10; Bal-Tec AG, Liechtenstein) at 210 MPa. Applying such a high pressure decreases the cooling rates required to avoid the formation of ice crystals, retaining water in the amorphous state (vitrification), thus allowing the preparation of thicker specimens that are better preserved (Studer et al., 2008). The frozen specimens were then mounted on a specialized sample table under liquid nitrogen, and transferred by a high vacuum cryo-transfer shuttle (VCT100; Bal-Tec) to a freeze-fracture system (BAF060; Leica) where it was kept at −170 °C. In the BAF060 chamber the sandwiches were split open using a cooled knife. The specimens were transferred under vacuum and at cryogenic temperature by the VCT100 shuttle, precooled with liquid nitrogen, to the precooled stage of the HR-SEM for imaging.

In the drop plunging method, a 3 μL drop of suspended cells is set on top of a special planchette maintaining its droplet shape and is manually plunged into liquid ethane, after which it is set on top

Please cite this article in press as: Koifman, N., et al. A direct-imaging cryo-EM study of shedding extracellular vesicles from leukemic monocytes. J. Struct. Biol. (2017), http://dx.doi.org/10.1016/j.jsb.2017.02.004

of a specialized sample table. The frozen droplets are transferred into the BAF060 freeze fracture system, where they are fractured by a rapid stroke from a cooled knife, exposing the inner part of the drop. They are then transferred into the pre-cooled HR-SEM as described above. Ideally, imaging is performed as close as possible to the drop surface, where cooling rate should be maximal.

2.3. Cryo-TEM

Cryogenic transmission electron microscopy (cryo-TEM) imaging was performed either by a Phillips CM120 or an FEI T12 G^2 electron microscopes, operated at 120 kV. Specimens were transferred into an Oxford CT-3500 cryo-holder (Philips TEM) or a Gatan 626DH (FEI TEM) cryo-holder, and equilibrated below −175 °C. Specimens were examined using a low-dose imaging procedure to minimize electron-beam radiation damage. Images were recorded digitally by a Gatan Multiscan 791 cooled CCD camera (Philips CM120), or a Gatan US 1000 high-resolution CCD camera (Tecnai T12 G^2), using the DigitalMicrograph® software.

Cryo-TEM specimens were prepared in a controlled environment vitrification system (CEVS) (Bellare et al., 1988). Since the system under study is aqueous, preparation was done in the temperature-controlled chamber with humidity at saturation, to prevent evaporation of volatiles (Talmon, 2015). Temperature was kept constant at 25 °C. A drop (~3 μL) of sample was placed within the CEVS on a carbon-coated perforated polymer film, supported on a 200 mesh TEM grid, mounted on a tweezer. The drop was turned into a thin film (preferably less than 300 nm) by blotting away excess solution with a filter paper-covered metal strip. The grid was then plunged quickly into liquid ethane at its freezing point (−183 °C). Prior to specimen preparation, grids were plasma etched in a PELCO EasiGlow glow-discharger (Ted Pella Inc., Redding, CA) to increase their hydrophilicity.

2.4. Nanoparticle tracking analysis (NTA)

Dilute suspensions of EVs were analyzed by nanoparticle tracking analysis on a NanoSight NS500 (Amesbury, U.K.) equipped with a 642 nm red laser module and on an NS300 equipped with a 532 nm green laser module. The NTA principle of operation is such that a laser light is passed through a prism edged glass flat to the sample chamber containing the EVs solution. The laser light is scattered from the vesicles, and owing to the angle of incidence and the refractive index of the glass flat it emerges from the sample with an intense signal. The refracted light is detected by a Hamamatsu A11893-01 scientific CMOS camera, operating at 25 frames per second. To achieve the optimal concentration range for NanoSight analysis (10^6–10^9 particles per ml) samples were diluted with PBS, 20–200 times, depending on the experiment, to a final sample volume of 1 mL. Each sample was studied five times by a 60 second video at a camera level between 14 and 16. Each video was analyzed by the NTA software (NTA 3.1, NanoSight Ltd.), which identifies the moving particles above a user-defined threshold (between 4 and 8 in this study), and then tracks their individual movement on a frame-by-frame basis, thus tracking their Brownian motion. The distance displaced by each particle is used for the calculation of its diffusion coefficient (D), which at a known temperature and viscosity can be used for the extraction of the sphere-equivalent hydrodynamic diameter from the Stokes-Einstein equation:

$$D = \frac{TK_B}{3\pi\eta d} \rightarrow d = \frac{TK_B}{3\pi\eta D}$$

where T is the temperature of the solvent in kelvin, K_B is Boltzmann's constant, η is the viscosity and d is the hydrodynamic diameter. Each analyzed video resulted in a mean, mode, and standard deviation values of particle diameter together with an estimate of particle concentration (Dragovic et al., 2011; Gercel-Taylor et al., 2012). All measurements were performed at 25 °C.

2.5. Flow cytometry for apoptosis

Apoptosis was measured by TdT-mediated dUTP Nick End Labeling (TUNEL) assay (In Situ Cell Detection Kit, Fluorescein; Roche, Germany) according to the kit instructions. In addition, in another assay, cells were stained by Annexin V-Fluorescein isothiocyanate (FITC) and propidium iodide (PI) (MEBCYTO® Apoptosis Kit, MBL international corporation, Massachusetts, U.S.A).

Following each of the above assays, cells were analyzed by flow cytometry on an BD-LSR-II, equipped with a 488 nm laser and a 505 nm long pass dichroic mirror and 530/30 bandpass filter directing FITC signal to the appropriate detector, and a 550 nm long pass dichroic mirror and 575/26 bandpass filter for isolating PI signal to the appropriate detector.

3. Results and discussion

3.1. Unstimulated cells specimens prepared by manual drop plunging vs. HPF

Comparing the different stimulation conditions was essential to establish our ability to recognize different degrees of shedding. Therefore, we initially imaged THP1 cells incubated in serum-complemented RPMI medium with no stimulation. Most cell membranes did not exhibit major blebs, and were fairly smooth and continuous. When comparing our specimens prepared by high pressure freezing (HPF) (Fig. 1A, C-D) to specimens prepared by manual drop plunging (Fig. 1B), we notice that although cells were visible, intact, and cell organelles were fairly well preserved by the drop method, HPF showed superior results, with fewer freezing artifacts and higher quality of preservation of inner and outer cellular nanostructures. In both preparation methods, some of the fractured cells exposed the cytoplasm and nucleus, and some remained whole, allowing an outer view of their membrane (Figs. 1D, 2E and 3B). Some of the interesting cellular features are the nucleus double membrane, which is observed either as it was partially removed or in a cross-section view (Figs. 1A and B, respectively), the nuclear pores (Fig. 2F), mitochondria (arrows, Fig. 2A) and in some other cellular cross-sections the endoplasmic reticulum and Golgi vesicles were identified (not shown). This emphasizes that since the cell is randomly fractured, each fracture may expose a different sampler of its components.

3.2. Cells exhibit different morphologies due to LPS or starvation stimulations

It is known that shedding of vesicles occurs under different types of stimulation, thus, we compared the extent of blebbing after LPS incubation and under starvation conditions. Cells after 4 h of LPS incubation showed a high degree of blebbing (Fig. 2A-E), which ranged in size, but was evident on most cells imaged. EV sizes ranged from as low as ~70 nm, and exceeded 1 μm, while the mean diameter ranged between 250 and 400 nm. This is the expected size of cell-membrane shed vesicles. EVs were mostly round or slightly elliptic in shape, which fits well with the EV morphology imaged by cryo-TEM (Fig. 4 below). Imaging of whole cells showed blebbing occurring across the whole membrane (Fig. 2E), while the cross-sections of fractured cells, verified the fact that the observed protrusions originated in fact from the changing curvature of the membrane. Different stages of shedding are visible, as

Please cite this article in press as: Koifman, N., et al. A direct-imaging cryo-EM study of shedding extracellular vesicles from leukemic monocytes. J. Struct. Biol. (2017), http://dx.doi.org/10.1016/j.jsb.2017.02.004

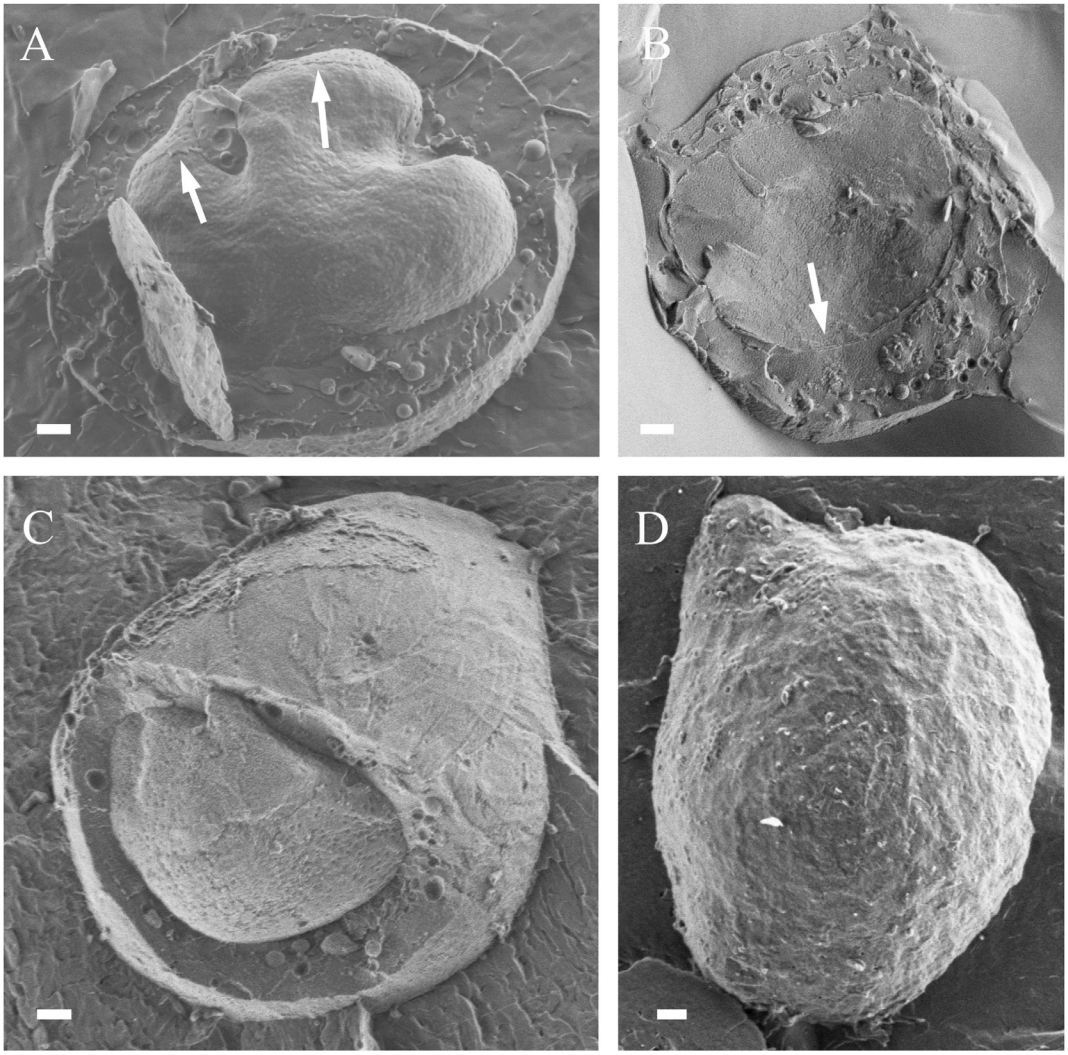

Fig. 1. Cryo-SEM of unstimulated THP1 cells. Specimens prepared by HPF (A, C-D) and by the drop method (B); no significant blebbing or extracellular vesicles are evident. The partially removed nuclear membrane is visible (arrows, A) and its cross-section (arrow, B). (C) A combined view of the cell, in which only parts of the membrane and the cytoplasm were removed, exposing the nucleus and organelles, while the rest of the unfractured membrane is visible. (D) A whole cell, with intact membrane. Bars = 1 μm.

membrane curvature increases, until the EV is finally pinched off and released (arrowheads in Fig. 2A & B, and arrow in Fig. 2B, respectively). Since the imaged cells are thermally fixed, in some cases we cannot determine unambiguously whether a vesicle is released by shedding or exocytosis, and possibly it may even be a vesicle that has been shed by a different cell, entering another cell by endocytosis. Such is the case in the arrow-labeled vesicle in Fig. 2D. This vesicle is fractured, exposing the fact that it is set in what might be a tunnel in which it travels towards its release. This is different than the mechanism we observed in Fig. 2A and B, where the curving membrane did not contain an inner vesicle, only the proximate cytoplasm, which may contain other cellular components, such as proteins and miRNA. However, the existence of a whole vesicle in the protruding membrane can also be related to the release mechanism of exosomes, if this vesicle is a multivesicular (MVB) body, for example. Compared to the cell-membrane shedding process, events such as the one described above, were rarely observed. Some of the shed EVs were observed in the proximity of the blebbing cells (Fig. 2C, D, & E), some of which remained whole, and some were removed during the specimen preparation procedure.

By increasing incubation time to 16 h we tried to address the question whether blebbing is a continuous process, which takes place as long as the cells are exposed to LPS. However, cells showed little to no blebbing after that period (Fig. 2F). Membranes were similar to the ones of unstimulated cells, and no effects of the LPS exposure were evident in the continuous membranes imaged. We did, however, spot in the vicinity of the cells vesicles that may have been shed earlier in the process. Thus, we may assume that after 16 h of incubation the cells had already passed the shedding stage, and that for the purposes of studying the shedding process, a 4-h incubation is sufficient.

In comparison to cell behavior during LPS incubation, cells that were incubated under starvation conditions (serum-free medium) exhibited different features on their membrane and in their inner morphology. We imaged cells after 24-h starvation and cells after 48-h starvation. While both exhibited a decreased level of blebbing compared to the LPS-stimulated cells, the morphology of protrusions observed on their membranes differed significantly from the LPS-stimulated cells. After 24 h of starvation only a little blebbing was observed on cells (Fig. 3A and Fig. 3B). Blebs were only slightly sticking out of the membrane (Fig. 3A), and we did not observe the EVs at their different shedding stages, since blebbing was not prevalent (Fig. 3B). Some of the protrusions had a more elongated and pointy shape, unlike the round vesicular protrusions observed in the LPS-stimulated cells. The elongated, pointed

Please cite this article in press as: Koifman, N., et al. A direct-imaging cryo-EM study of shedding extracellular vesicles from leukemic monocytes. J. Struct. Biol. (2017), http://dx.doi.org/10.1016/j.jsb.2017.02.004

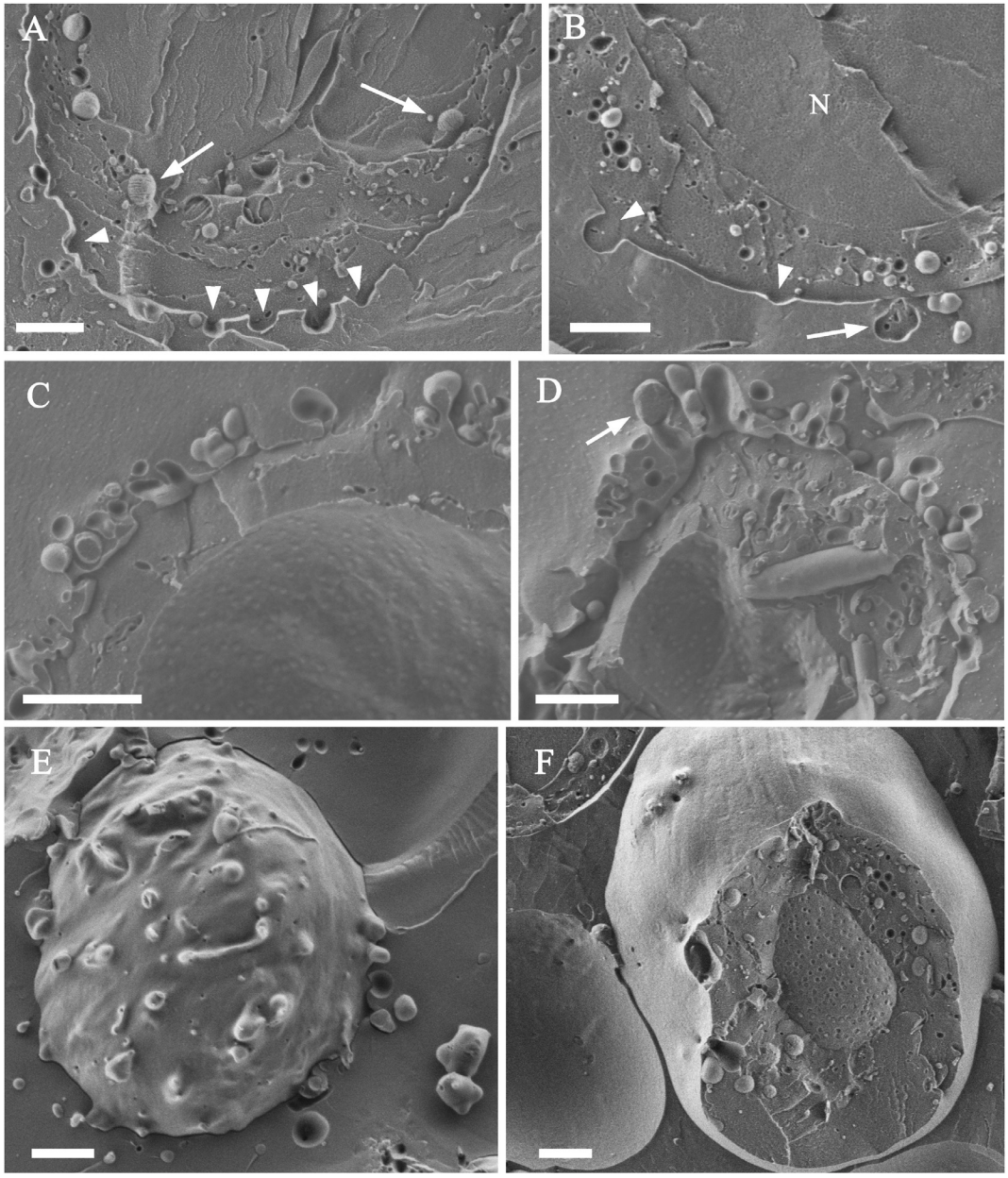

Fig. 2. Cryo-SEM of THP1 cells incubated with LPS for 4 h (A–E), showing extensive blebbing on the membrane, either in cross-section view of fractured cells (A-D), or an outer view of whole cells (E). (A-B) Different stages of membrane curvature are evident (arrowheads), as well as an EV that is pinched-off (arrow). Mitochondria are clearly visible in the fractured cell (arrows in A), and the cell nucleus (N) is labeled for clarity in (B). (C) A cell showing a high degree of blebbing at different stages of the process. (D) A vesicle removed through a membrane channel is exposed due to the fracture (arrow). (C-E) Some shed microparticles are seen in the proximity of the blebbing cells. The membrane seems to have a smooth morphology, except in the areas where EVs are blebbing. LPS incubation for 16 h (F) showed very little or no blebbing, with relatively smooth-appearance of membranes. Nuclear pores are clearly visible due to the excellent preservation of cells by the HPF preparation. Bars = 2 μm.

protrusions were highly prevalent in the 48-h starvation cells. These nanostructures appeared both on whole cells (Fig. 3D) and in fractured cells (Fig. 3C and E), where it was verified that they stem from the cell membrane. Some of the 48-h starved cells also showed a crumpled appearance of the nucleus of some cells (Fig. 3C).

Direct cryo-TEM imaging of EVs isolated from cells following LPS incubation (Fig. 4A & B), or starvation conditions (Fig. 4C & D), did not suggest any striking morphological differences. In both cases, they were mostly round in shape and highly heterogeneous in diameter. The micrographs in Fig. 4 show the variety of morphologies that were observed in samples from both types of isolations. One can differentiate between smooth versus granular EVs (Fig. 4A), in which the granularity protrudes from the EVs membrane. The EVs in Fig. 4C and D seem to encapsulate some cellular material, while the large EV in Fig. 4B may be a multivesicular body encapsulating exosomes. An existing limitation of cryo-TEM that should be considered is that film thickness is up to several hundreds of nanometers, thus, large EVs (1 μm) may be excluded during specimen preparation procedure, which includes the blotting of a drop of sample. In addition, though our isolation protocol includes only a 20,000*g* centrifugation step, which should potentially leave out tiny vesicles, vesicles that are smaller than 100 nm are visible throughout our samples.

Because cryo-TEM is not truly quantitative, we used NTA for the comparison of both concentration and mean diameter of EVs isolated after the two stimulation types. While analysis of cryo-TEM micrographs did not reveal striking differences, NTA measure-

Please cite this article in press as: Koifman, N., et al. A direct-imaging cryo-EM study of shedding extracellular vesicles from leukemic monocytes. J. Struct. Biol. (2017), http://dx.doi.org/10.1016/j.jsb.2017.02.004

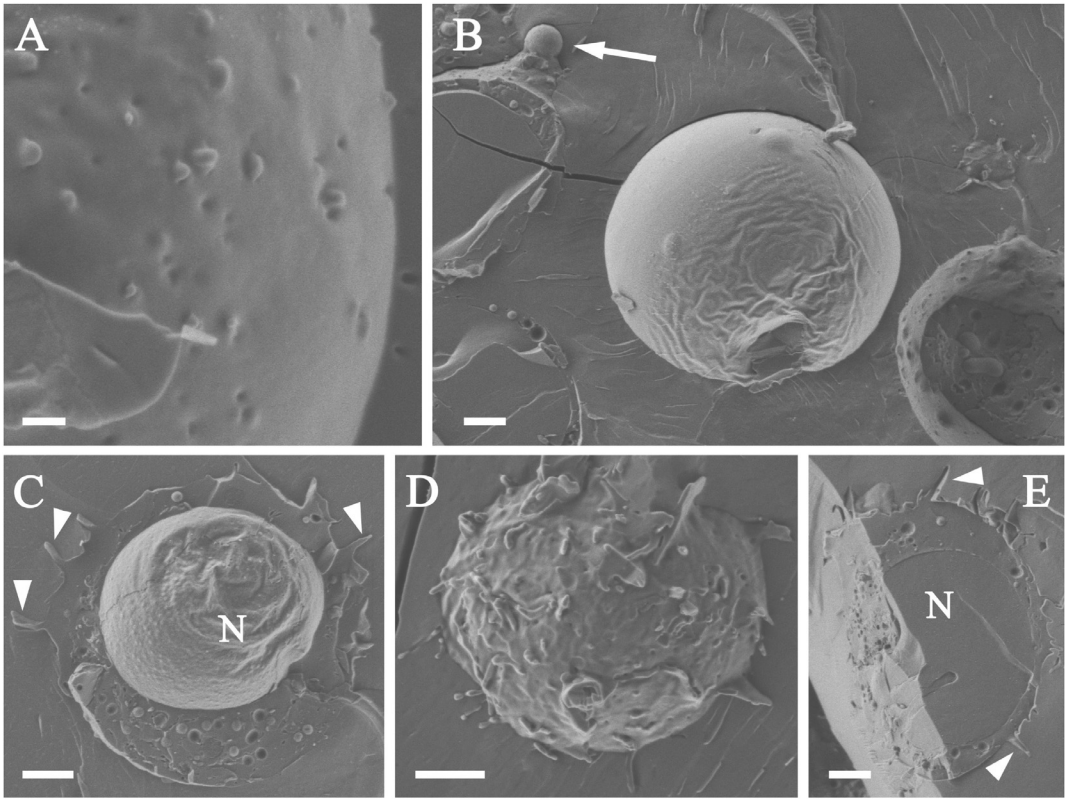

Fig. 3. Cryo SEM of THP1 cells incubated under starvation conditions for 24 h (A-B) and for 48 h (C-E). (A) High magnification image of the cell membrane showing moderate blebbing, smaller than 200 nm in diameter; most blebs protrude only partially compared to blebs observed after LPS stimulation. (B) The cell in the center has a wrinkled membrane with blebbing starting at several positions. The cell on the left shows a large bleb, ~850 nm in diameter (arrow). (C) A cross-section of a cell after 48-h starvation, membrane is disrupted with elongated nanostructures (arrowheads); nucleus (N) has a wrinkled morphology possibly indicating its shrinking. Nuclear membrane is partially removed and nuclear pores are visible. (D) An entire cell after 48-h starvation; membrane is highly disrupted with elongated protruding nanostructures. (E) A cell fractured along two perpendicular planes, exhibiting elongated protrusions (arrowheads) all-over the membrane. Fractured nucleus is marked (N). Bars A = 400 nm, B = 1 μm, C-E = 2 μm.

ments suggested otherwise. In agreement with our cryo-SEM results, NTA analysis showed an increase concentration of EVs isolated from LPS stimulated cells. Comparison was performed on EVs isolated in the same isolation session. Because concentrations of EVs may vary from one isolation session to another, we defined a normalized parameter, C_{rel}, which is the ratio between the concentrations of EVs isolated from LPS stimulated cells (C_{LPS}) and EVs isolated from starvation stimulated cells (C_{Starv}).

$$C_{rel} = \frac{C_{LPS}}{C_{Starv}}$$

The mean value of Crel was found to be 4.34 with a relative standard deviation of 89%. The values of Crel range between 1.2 and 14, with a median value of 2.15. It is clear from these results that the concentration of LPS-stimulated EVs is consistently higher than the [I1] concentration of starvation EVs (Supplementary Fig. S1). EVs concentrations were also compared to EVs isolated from unstimulated cells, as shown in Table 1. The ratio of LPS to unstimulated EVs was 1.49, while the ratio between starvation and unstimulated EVs was 0.24. These results emphasize the elevated shedding response due to LPS stimulation, while implying a decreased shedding response during the starvation stimulation. Another interesting result was the comparison between average particle diameters as measured by NTA, demonstrating starvation-stimulated EVs are larger on the average in diameter than LPS-stimulated EVs. The mean diameter measured for LPS induced EVs was 153 nm, compared to 213 nm for starvation induced EVs (Fig. 5A). Both resulted in a fairly large relative standard deviation of 45% and 46% for LPS and starvation induced EVs, respectively, which emphasizes the widespread distribution of diameters in EV samples in general. Additionally, most vesicles were smaller than 200 nm, with a large peak around 100 nm (Fig. 5B & C), for both types of stimulations. If we perform an unpaired *t*-test on the mean diameter values, we obtain a two-tailed P value of 0.0015, which is highly statistically significant. NTA is limited in the analysis of highly heterogeneous particle mixtures. This is as a result of focus and detection threshold settings, which are different for large and small particles that are found in the EVs samples naturally. Though we do detect particles as large as 500 and 600 nm in diameter, they are fewer in number compared to the small particles analyzed by NTA. Taking this limitation into account, we use a combination of characterization techniques, namely, cryo-TEM, cryo-SEM and NTA to establish a complete view of the size range of particles, though it is indeed possible that the lion's share of vesicles is smaller than 200 nm.

As far as we know, this is the first time the shedding process is followed by direct imaging at such a high resolution, revealing some striking differences in terms of cellular morphology between different types of stimulations. The different stages of blebbing and shedding are shown with great detail, and agree with the structural models that were suggested in previous studies (Piccin et al., 2007). Most EVs observed by cryo-SEM were in the size range attributed to microvesicles, which are cell-membrane shed. Cryo-TEM provided images of a wider range of EVs, thus complementing the cellular point of view.

Please cite this article in press as: Koifman, N., et al. A direct-imaging cryo-EM study of shedding extracellular vesicles from leukemic monocytes. J. Struct. Biol. (2017), http://dx.doi.org/10.1016/j.jsb.2017.02.004

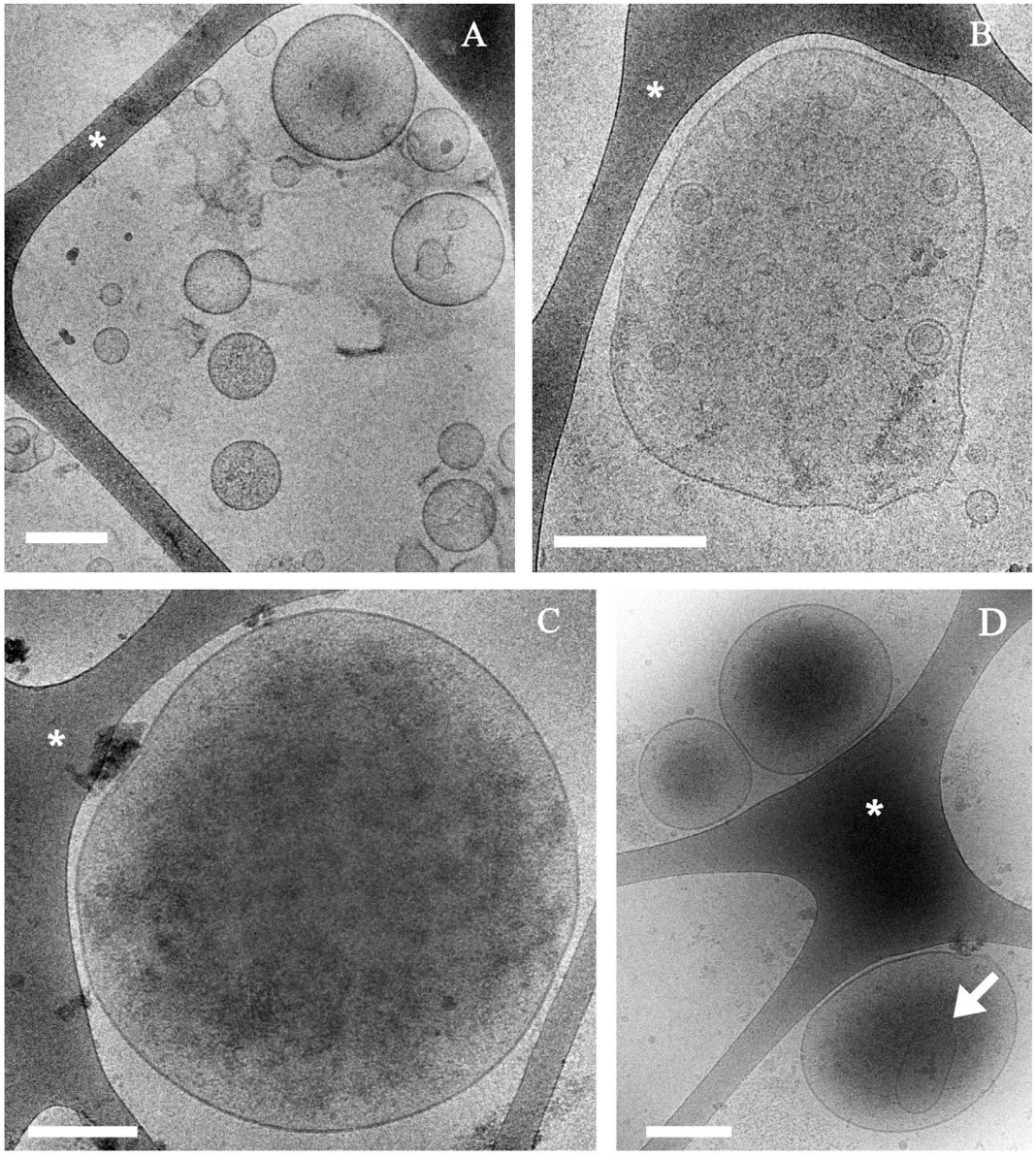

Fig. 4. Cryo-TEM images of extracellular vesicles isolated from THP1 cells. (A-B) EVs after 4-h incubation with LPS, where granulated versus smooth EVs are visible, as well as a possible MVB containing smaller vesicles, possibly exosomes. (C-D) EVs after 48-h incubation under starvation conditions. A large vesicle containing cellular material (C), and (D) smaller vesicles also containing cellular material and even smaller vesicles (arrow). The high heterogeneity in size, texture and content is evident in both types of samples; no distinct differences are identified between them. Bars = 200 nm. Perforated carbon film is indicated by asterisks.

Table 1
Concentration Ratios as measured by NTA.

Compared Samples	$\frac{C_{LPS}}{C_{Unstimulated}}$	$\frac{C_{Starvation}}{C_{Unstimulated}}$	$\frac{C_{LPS}}{C_{Starv}}$
Ratio	1.49	0.24	4.34

Our present work shows clear differences in the morphologies of cells under different stimulation types, which are commonly used for inducting EVs shedding. Aharon et al. (Aharon et al., 2008) have demonstrated the increased levels of endosomal sorting protein, Tsg101, on EVs isolated from cells stimulated by LPS and Ca ionophore, as compared to EVs isolated from cells after 20 h starvation. Though there are studies that show that TSG101 can be expressed on membrane-shed microparticles (Nabhan et al., 2012), this protein is typically found on exosomes, which are released from MVBs, and are estimated to be smaller in diameter (Ekström et al., 2013). Thus, it is possible that LPS induces the elevated release of exosomes, which is also manifested in a smaller average EV diameter, considering it is a heterogeneous mixture of both exosomes and cell-membrane shed EVs.

Conversely, our observation of cells after 48-h starvation, including elongated membrane protrusions, general shrinkage of the cell, together with nuclear condensation, are morphological features associated with cells undergoing apoptosis (Elmore, 2007). In late stages of apoptosis, large membrane blebs appear, which are eventually shed from the cell, and are known as apoptotic bodies. *In vivo* the shed apoptotic bodies are phagocytosed by other immune cells, and are degraded by phagolysosomes (Elmore, 2007). To validate or refute the apoptotic state of the cells, we applied both TUNEL assay and Annexin-V/PI staining to the cells, which both showed negative results for apoptosis. Combining this result with the NTA concentration measurements, which indicate a decrease in cellular shedding upon starvation, introduces the

Please cite this article in press as: Koifman, N., et al. A direct-imaging cryo-EM study of shedding extracellular vesicles from leukemic monocytes. J. Struct. Biol. (2017), http://dx.doi.org/10.1016/j.jsb.2017.02.004

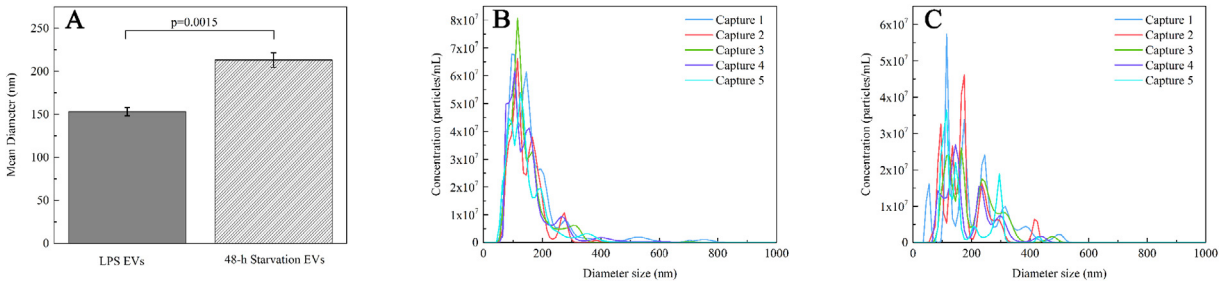

Fig. 5. (A) Mean diameter of EV samples isolated from LPS-stimulated cells (■) or from starvation-stimulated cells (/). The values presented are averaged over 13 measured samples. P value is 0.0015 < 0.05, which indicates a high level of statistical significance. An example of a typical NTA measurement of (B) EVs isolated from LPS-stimulated cells and (C) EVs isolated from starvation-stimulated cells. Each session is composed of 5 60-s long captures. One can notice the increased heterogeneity of the starvation sample expressed by the graph distribution and the higher peaks at higher diameters.

possibility that starvation stimulation leads to cell arrest rather than to apoptosis (Chen et al., 2000; Shin et al., 2008). Based on these results we cannot attribute unambiguously the unique morphological features of starved cells to apoptosis.

The effects of LPS exposure on cellular behavior and gene expression of monocytes have been a subject for research. Porta et al. (Landmann et al., 1996) showed that LPS affects the expression of membrane-bound CD14, a glycosylphosphatidylinositol (GPI)-linked membrane glycoprotein, which serves as a receptor for LPS and LPS-binding protein complexes. Following up to 15 h of exposure, membrane CD14 levels decreased, while longer incubation times of up to 44 h lead to increased expression of membrane CD14. In another study, while short exposure (4 h) of monocytes to LPS led them into a classical (M1) activation state, elongated exposure time (24 h) rendered them "LPS-tolerant", expressing an alternatively-activated (M2) macrophage phenotype (Porta et al., 2009). Our results also suggest a difference between the short and the long-term effect of LPS incubation, showing that blebbing is prominent after 4 h, but is rarely evident after 16-h. That may be related to the change in their immune response, or to other effects rendered by prolonged LPS exposure, which are related to the uptake of LPS by the stimulated cells.

It is interesting that although cells showed a different morphology, we could not identify distinct differences between the shed EVs morphologies by cryo-TEM, which emphasizes the elusiveness in the study of EVs in general regarding their nanostructure and composition. However, since cellular morphology complemented with NTA results indicating differences both in average diameter and in EVs concentration resulting from the different stimulation types, one should keep in mind that this may affect the EV type (exosomes, MPs, or apoptotic bodies) shed along with their proteomic content. That is, of course, a point for further investigation, which we hope to address by the development of an immunogold labeling protocol, which will be applied in cryo-SEM as well as on cryo-TEM specimens, thus elucidating the membrane composition of the shed vesicles.

Cryo-SEM allows direct imaging of cells as close as possible to their morphology at room temperature, with no additional fixative chemicals of any sort. Thus, we are confident that the membrane effects we observe in our specimens are indeed a result of processes undergoing in the cells, not artifacts. However, one should keep in mind that because cryo-SEM specimens are physically fixed at a certain point in time, deductions regarding dynamic processes should be carried out with extra caution. We image our cells with no additional coating, using a relatively low acceleration voltage, however, cells are relatively sensitive to electron beam radiation, which induces rapid radiation damage at high magnifications. This limits our ability to identify EVs that are tens of nanometers in size shedding from the cells by cryo-SEM, although we do identify them by cryo-TEM after isolation.

4. Conclusions

Our results suggest differences in the nature of the EVs released from the two types of stimulation. It is possible that the cells undergoing LPS incubation release more exosomes, resulting in the observed decrease in average EV diameter. The decrease in EV concentration isolated from starved cells may be due to cellular arrest, not necessarily due to apoptosis. The two stimulation processes we used in this study are *in-vitro* procedures. EVs shedding from monocyte cells was induced by cells exposed to starvation conditions (used as a model for "stress") or to LPS. While "starvation" can be performed only *in-vitro*, infection with LPS, endotoxin from the outer membrane of Gram-negative bacteria is very common, and thus simulates *in-vivo* processes. It can cause variety of pathologies from mild fever to lethal septic shock, organ failure, and death (Hawkins et al., 2004). Sepsis is characterized by activation of the immune system (Zhang et al., 2016); the onset of septic shock occurs due to the over-activation of monocytes (Oliva-Martin et al., 2016) that can result in massive shedding of EVs, as demonstrated in the current study. Our study provides an innovative high-resolution view of the process of shedding and its released EVs, suggeting that while certain stimulations have an intensifying effect on shedding level, others may have an inhibiting effect. Our results open a path for further investigation, which will include an immunogold labeling assay of the shedding cells by cryo-SEM, and of the shed EVs by cryo-TEM, in an attempt to elucidate the lipid composition and its relation to the observed morphology.

Acknowledgments

We thank Prof. Alejandro Sosnik and Ms. Maya Menkar for their assistance with the NS500 NanoSight measurements. We thank Prof. Avi Schroeder for kindly allowing us to culture cells in his lab. We thank Dr. Janna Shainsky for her generous, useful, and kind assistance at all times. A special thank you to Dr. Eyal Shimoni for his kind assistance and guidance regarding the HPF work, and for fruitful discussions of cryo-SEM specimen preparation. Finally, we would like to thank Dr. Gal Mor Khalifa and Dr. Michael Kerschnitzki for their kind support with the HPF work at the Weizmann Institute of Science.

NK thanks the Israeli Ministry of Science, Technology and Space for the Aloni Scholarship. This research was funded in part by the Technion Russell Berrie Nanotechnology Institute (RBNI) through

its Nevet Program. The EM work was performed at the Laboratory of Electron Microscopy of Soft Materials, supported by the RBNI.

Appendix A. Supplementary data

Supplementary data associated with this article can be found, in the online version, at http://dx.doi.org/10.1016/j.jsb.2017.02.004.

References

Aharon, A., Tamari, T., Brenner, B., 2008. Monocyte-derived microparticles and exosomes induce procoagulant and apoptotic effects on endothelial cells. Thromb. Haemost. 100, 878–885.

Alexander, C., Rietschel, E.T., 2001. Bacterial lipopolysaccharides and innate immunity. J. Endotoxin Res. 7, 167–202.

Arraud, N., Linares, R., Tan, S., Gounou, C., Pasquet, J.-M., Mornet, S., Brisson, A.R., 2014. Extracellular vesicles from blood plasma: determination of their morphology, size, phenotype and concentration. J. Thromb. Haemost. 12, 614–627.

Atkin-Smith, G.K., Tixeira, R., Paone, S., Mathivanan, S., Collins, C., Liem, M., Goodall, K.J., Ravichandran, K.S., Hulett, M.D., Poon, I.K.H., 2015. A novel mechanism of generating extracellular vesicles during apoptosis via a beads-on-a-string membrane structure. Nat. Commun. 6, 7439.

Bellare, J.R., Davis, H.T., Scriven, L.E., Talmon, Y., 1988. Controlled environment vitrification system: an improved sample preparation technique. J. Electron Microsc. Tech. 10, 87–111.

Castellana, D., Toti, F., Freyssinet, J.-M., 2010. Membrane microvesicles: macromessengers in cancer disease and progression. In: Pap. Abstr. 5th Int. Conf. Thromb. Hemost. Issues Cancer 125, Suppl, S84–S88.

Chahed, S., Leroyer, A.S., Benzerroug, M., Gaucher, D., Georgescu, A., Picaud, S., Silvestre, J.-S., Gaudric, A., Tedgui, A., Massin, P., Boulanger, C.M., 2010. Increased vitreous shedding of microparticles in proliferative diabetic retinopathy stimulates endothelial proliferation. Diabetes 59, 694–701.

Chen, C., Lin, H., Karanes, C., Pettit, G.R., Chen, B.D., 2000. Human THP-1 monocytic leukemic cells induced to undergo monocytic differentiation by Bryostatin 1 are refractory to proteasome inhibitor-induced apoptosis. Cancer Res. 60.

Cocucci, E., Racchetti, G., Meldolesi, J., 2009. Shedding microvesicles: artefacts no more. Trends Cell Biol. 19, 43–51.

Crompot, E., Van Damme, M., Duvillier, H., Pieters, K., Vermeesch, M., Perez-Morga, D., Meuleman, N., Mineur, P., Bron, D., Lagneaux, L., Stamatopoulos, B., 2015. Avoiding false positive antigen detection by flow cytometry on blood cell derived microparticles: the importance of an appropriate negative control. PLoS One 10, e0127209.

Dragovic, R.A., Gardiner, C., Brooks, A.S., Tannetta, D.S., Ferguson, D.J.P., Hole, P., Carr, B., Redman, C.W.G., Harris, A.L., Dobson, P.J., Harrison, P., Sargent, I.L., 2011. Sizing and phenotyping of cellular vesicles using Nanoparticle Tracking Analysis. Nanomedicine 7, 780–788.

Ekström, K., Omar, O., Granéli, C., Wang, X., Vazirisani, F., Thomsen, P., 2013. Monocyte exosomes stimulate the osteogenic gene expression of mesenchymal stem cells. PLoS One 8, e75227.

Eldh, M., Ekström, K., Valadi, H., Sjöstrand, M., Olsson, B., Jernås, M., Lötvall, J., 2010. Exosomes communicate protective messages during oxidative stress; possible role of exosomal shuttle RNA. PLoS One 5, e15353.

Elmore, S., 2007. Apoptosis: a review of programmed cell death. Toxicol. Pathol. 35, 495–516.

Gercel-Taylor, C., Atay, S., Tullis, R.H., Kesimer, M., Taylor, D.D., 2012. Nanoparticle analysis of circulating cell-derived vesicles in ovarian cancer patients. Anal. Biochem. 428, 44–53.

Gould, S.J., Raposo, G., 2013. As we wait: coping with an imperfect nomenclature for extracellular vesicles. J. Extracell. Vesicles.

Hargett, L.A., Bauer, N.N., 2013. On the origin of microparticles: from "platelet dust" to mediators of intercellular communication. Pulm. Circ. 3, 329–340.

Hawkins, L.D., Christ, W.J., Rossignol, D.P., 2004. Inhibition of endotoxin response by synthetic TLR4 antagonists. Curr. Top. Med. Chem. 4, 1147–1171.

Hedlund, M., Nagaeva, O., Kargl, D., Baranov, V., Mincheva-Nilsson, L., 2011. Thermal- and oxidative stress causes enhanced release of NKG2D ligand-bearing immunosuppressive exosomes in leukemia/lymphoma T and B cells. PLoS One 6, e16899.

Heijnen, H.F.G., Schiel, A.E., Fijnheer, R., Geuze, H.J., Sixma, J.J., 1999. Activated platelets release two types of membrane vesicles: microvesicles by surface shedding and exosomes derived from exocytosis of multivesicular bodies and a-granules. Blood 94, 3791–3799.

Hugel, B., Martínez, M.C., Kunzelmann, C., Freyssinet, J.M., 2005. Membrane microparticles: two sides of the coin. Physiology 20, 22–27.

Issman, L., Brenner, B., Talmon, Y., Aharon, A., 2013. Cryogenic transmission electron microscopy nanostructural study of shed microparticles. PLoS One 8, e83680.

Jaiswal, R., Luk, F., Dalla, P.V., Grau, G.E.R., Bebawy, M., 2013. Breast cancer-derived microparticles display tissue selectivity in the transfer of resistance proteins to cells. PLoS One 8.

Katsuda, T., Kosaka, N., Ochiya, T., 2014. The roles of extracellular vesicles in cancer biology: toward the development of novel cancer biomarkers. Proteomics 14, 412–425.

Katzenell, S., Shomer, E., Zipori, Y., Zylberfisz, A., Brenner, B., Aharon, A., 2012. Characterization of negatively charged phospholipids and cell origin of microparticles in women with gestational vascular complications. Thromb. Res. 130, 479–484.

Lai, C.P., Kim, E.Y., Badr, C.E., Weissleder, R., Mempel, T.R., Tannous, B.A., Breakefield, X.O., 2015. Visualization and tracking of tumour extracellular vesicle delivery and RNA translation using multiplexed reporters. Nat. Commun. 6, 7029.

Landmann, R., Knopf, H.P., Link, S., Sansano, S., Schumann, R., Zimmerli, W., 1996. Human monocyte CD14 is upregulated by lipopolysaccharide. Infect. Immun. 64, 1762–1769.

Meziani, F., Tesse, A., Andriantsitohaina, R., 2008. Microparticles are vectors of paradoxical information in vascular cells including the endothelium: role in health and diseases. Pharmacol. Rep. 60, 75–84.

Minciacchi, V., Freeman, M.R., Di Vizio, D., 2015a. Extracellular vesicles in cancer: exosomes, microvesicles and the emerging role of large oncosomes. Semin. Cell Dev. Biol. 40, 41–51.

Minciacchi, V., You, S., Spinelli, C., Morley, S., Zandian, M., Aspuria, P.-J., Cavallini, L., Ciardiello, C., Sobreiro, M.R., Morello, M., Kharmate, G., Jang, S.C., Kim, D.-K., Hosseini-Beheshti, E., Guns, E.T., Gleave, M., Gho, Y.S., Mathivanan, S., Yang, W., Freeman, M.R., Vizio, D.Di., 2015b. Large oncosomes contain distinct protein cargo and represent a separate functional class of tumor-derived extracellular vesicles. Oncotarget 6, 11327–11341.

Nabhan, J.F., Hu, R., Oh, R.S., Cohen, S.N., Lu, Q., 2012. Formation and release of arrestin domain-containing protein 1-mediated microvesicles (ARMMs) at plasma membrane by recruitment of TSG101 protein. Proc. Natl. Acad. Sci. U. S.A. 109, 4146–4151.

Oliva-Martin, M.J., Sanchez-Abarca, L.I., Rodhe, J., Carrillo-Jimenez, A., Vlachos, P., Herrera, A.J., Garcia-Quintanilla, A., Caballero-Velazquez, T., Perez-Simon, J.A., Joseph, B., Venero, J.L., 2016. Caspase-8 inhibition represses initial human monocyte activation in septic shock model. Oncotarget 7, 37456–37470.

Piccin, A., Murphy, W.G., Smith, O.P., 2007. Circulating microparticles: pathophysiology and clinical implications. Blood Rev. 21, 157–171.

Porta, C., Rimoldi, M., Raes, G., Brys, L., Ghezzi, P., Di Liberto, D., Dieli, F., Ghisletti, S., Natoli, G., De Baetselier, P., Mantovani, A., Sica, A., 2009. Tolerance and M2 (alternative) macrophage polarization are related processes orchestrated by p50 nuclear factor kappaB. Proc. Natl. Acad. Sci. U.S.A. 106, 14978–14983.

Redman, C.W.G., Sargent, I.L., 2007. Microparticles and immunomodulation in pregnancy and pre-eclampsia. In: Proc. 5th Int. Work. Reprod. Immunol. Immunol. Toler. Immunol. Preeclampsia, 76, pp. 61–67.

Shai, E., Varon, D., 2011. Development, cell differentiation, angiogenesis-microparticles and their roles in angiogenesis. Arterioscler. Thromb. Vasc. Biol. 31, 10–14.

Shedden, K., Xie, X.T., Chandaroy, P., Chang, Y.T., Rosania, G.R., 2003. Expulsion of small molecules in vesicles shed by cancer cells: association with gene expression and chemosensitivity profiles. Cancer Res. 63, 4331–4337.

Shin, J.-S., Hong, S.-W., Lee, S.-L.O., Kim, T.-H., Park, I.-C., An, S.-K., Lee, W.-K., Lim, J.-S., Kim, K.-I., Yang, Y., Lee, S.-S., Jin, D.-H., Lee, M.-S., 2008. Serum starvation induces G1 arrest through suppression of Skp2-CDK2 and CDK4 in SK-OV-3 cells. Int. J. Oncol. 32, 435–439.

Shomer, E., Katzenell, S., Zipori, Y., Sammour, R.N., Isermann, B., Brenner, B., Aharon, A., 2013. Microvesicles of women with gestational hypertension and preeclampsia affect human trophoblast fate and endothelial function. Hypertension 62, 893–898.

Studer, D., Humbel, B.M., Chiquet, M., 2008. Electron microscopy of high pressure frozen samples: bridging the gap between cellular ultrastructure and atomic resolution. Histochem. Cell Biol. 130, 877–889.

Sturk, A., Nieuwland, R., 2012. Cell-derived vesicles in health and disease. Ned. Tijdschr. voor Klin. Chemie en Lab. 37, 65–68.

Talmon, Y., 2015. The study of nanostructured liquids by cryogenic-temperature electron microscopy — a status report. J. Mol. Liq. 210, 2–8.

Théry, C., Zitvogel, L., Amigorena, S., 2002. Exosomes: composition, biogenesis and function. Nat. Rev. Immunol. 2, 569–579.

Tsimerman, G., Roguin, A., Bachar, A., Melamed, E., Brenner, B., Aharon, A., 2011. Involvement of microparticles in diabetic vascular complications. Thromb. Haemost. 106, 310–321.

van Der Pol, E., Hoekstra, A.G., Sturk, A., Otto, C., Van Leeuwen, T.G., Nieuwland, R., 2010. Optical and non-optical methods for detection and characterization of microparticles and exosomes. J. Thromb. Haemost. 8, 2596–2607.

van der Pol, E., Coumans, F.A.W., Grootemaat, A.E., Gardiner, C., Sargent, I.L., Harrison, P., Sturk, A., van Leeuwen, T.G., Nieuwland, R., 2014. Particle size distribution of exosomes and microvesicles determined by transmission electron microscopy, flow cytometry, nanoparticle tracking analysis, and resistive pulse sensing. J. Thromb. Haemost. 12, 1182–1192.

Zhang, X., Li, N., Shao, H., Meng, Y., Wang, L., Wu, Q., Yao, Y., Li, J., Bian, J., Zhang, Y., Deng, X., 2016. Methane limit LPS-induced NF-κB/ MAPKs signal in macrophages and suppress immune response in mice by enhancing PI3K/AKT/GSK-3β- mediated IL-10 expression. Nat. Publ. Gr.

Zomer, A., Maynard, C., Verweij, F.J., Kamermans, A., Schäfer, R., Beerling, E., Schiffelers, R.M., de Wit, E., Berenguer, J., Ellenbroek, S.I.J., Wurdinger, T., Pegtel, D.M., van Rheenen, J., 2015. In vivo imaging reveals extracellular vesicle-mediated phenocopying of metastatic behavior. Cell 161, 1046–1057.